Rates of Elementary Catalytic Steps for Different Metal Forms of the Family II Pyrophosphatase from *Streptococcus gordonii*†

Anton B. Zyryanov,‡ Alexander V. Vener,§ Anu Salminen,|| Adrian Goldman,⊥ Reijo Lahti,*,|| and Alexander A. Baykov*,‡

A. N. Belozersky Institute of Physico-Chemical Biology and School of Chemistry, Moscow State University, Moscow 119899, Russia, Division of Cell Biology, Linköping University, SE-581 85 Linköping, Sweden, Department of Biochemistry, University of Turku, FIN-20014 Turku, Finland, and Institute of Biotechnology, University of Helsinki, P.O. Box 56, FIN-00014 Helsinki, Finland

Received September 29, 2003

ABSTRACT: Soluble inorganic pyrophosphatases (PPases) form two nonhomologous families, denoted I and II, that have similar active-site structures but different catalytic activities and metal cofactor specificities. Family II PPases, which are often found in pathogenic bacteria, are more active than family I PPases, and their best cofactor is Mn^{2+} rather than Mg^{2+}, the preferred cofactor of family I PPases. Here, we present results of a detailed kinetic analysis of a family II PPase from *Streptococcus gordonii* (*sg*PPase), which was undertaken to elucidate the factors underlying the different properties of family I and II PPases. We measured rates of PP_i hydrolysis, PP_i synthesis, and P_i/water oxygen exchange catalyzed by *sg*PPase with Mn^{2+}, Mg^{2+}, or Co^{2+} in the high-affinity metal-binding site and Mg^{2+} in the other sites, as well as the binding affinities for several active-site ligands (metal cofactors, fluoride, and P_i). On the basis of these data, we deduced a minimal four-step kinetic scheme and evaluated microscopic rate constants for all eight relevant reaction steps. Comparison of these results with those obtained previously for the well-known family I PPase from *Saccharomyces cerevisiae* (Y-PPase) led to the following conclusions: (a) catalysis by *sg*PPase does not involve the enzyme-PP_i complex isomerization known to occur in family I PPases; (b) the values of k_{cat} for the magnesium forms of *sg*PPase and Y-PPase are similar because of similar rates of bound PP_i hydrolysis and product release; (c) the marked acceleration of *sg*PPase catalysis in the presence of Mn^{2+} and Co^{2+} results from a combined effect of these ions on bound PP_i hydrolysis and P_i release; (d) *sg*PPase exhibits lower affinity for both PP_i and P_i; and (e) *sg*PPase and Y-PPase exhibit similar values of k_{cat}/K_m, which characterizes the PPase efficiency in vivo (i.e., at nonsaturating PP_i concentrations).

Soluble inorganic pyrophosphatase (EC 3.6.1.1, PPase)[1] is a ubiquitous enzyme that hydrolyzes PP_i to P_i, thereby providing a thermodynamic pull for many biochemical processes that yield PP_i as a byproduct (e.g., nucleic acid and protein syntheses) (*1*, *2*). Soluble PPases comprise two families, denoted I and II (*3*, *4*). Family II is found only in bacteria and archaebacteria, often pathogenic, whereas family I is found in all types of organisms. The members of each family show a clear homology in amino acid sequence, but no homology exists between the families. Family I PPases are dimers or hexamers of identical subunits, whereas all family II PPases are homodimers.

The catalytic mechanism of family I PPases has been studied in detail from both the kinetic and the structural viewpoints (*2*, *5*−*7*). PP_i hydrolysis proceeds as a direct nucleophilic attack of a water molecule, activated by coordination with two metal ions (possibly converting it to a hydroxide ion) on the phosphorus of PP_i. Metal ions also shield the negative charges of the oxygen atoms of the electrophilic phosphate group, facilitating the approach of the nucleophile. Scheme 1 (*5*) describes the steps involved in catalysis by PPase from *Saccharomyces cerevisiae* (Y-PPase), the best-characterized family I PPase. The rate constants for most of the reaction steps in Scheme 1 are known (*5*), as are the X-ray structures of the resting enzyme (E) and two of the reaction intermediates (EPP and EP_2) (*6*, *8*). An important feature of Scheme 1, supported by ample kinetic evidence (*5*, *9*), is the reversible isomerization of the enzyme−substrate complex (steps k_A and k_B). According to recent kinetic (*10*) and X-ray crystallographic (*8*) data, a similar isomerization of the enzyme−substrate complex ($EP_2^* \rightleftarrows EP_2$) most likely occurs in the reverse reaction.

† This work was supported by grants from the Russian Foundation for Basic Research (03-04-48798); the Ministry of Industry, Science and Technologies of the Russian Federation (1706-2003-4); the Finnish Academy of Sciences (201611, 47513, 172168, and 178376); the Sigrid Juselius Foundation; the Royal Swedish Academy of Sciences; and The Swedish Research Council.

* To whom correspondence should be addressed. (A.A.B.) Tel: 095-939-5541. Fax: 095-939-3181. E-mail: baykov@genebee.msu.su. (R.L.)Tel: 358-2-333-6845. Fax: 358-2-333-6860. E-mail: reijo.lahti@utu.fi.

‡ Moscow State University.

§ Linköping University.

|| University of Turku.

⊥ University of Helsinki.

[1] Abbreviations: PPase, inorganic pyrophosphatase; P_i, inorganic phosphate; PP_i, inorganic pyrophosphate; *sg*PPase, *Streptococcus gordonii* inorganic pyrophosphatase; Y-PPase, yeast (*Saccharomyces cerevisiae*) inorganic pyrophosphatase.

10.1021/bi0357513 CCC: $27.50
Published on Web 12/31/2003

Scheme 1: Kinetic Scheme of Catalysis by Y-PPase

$$E \underset{k_2}{\overset{k_1}{\rightleftarrows}} EPP^* \underset{k_B}{\overset{k_A}{\rightleftarrows}} EPP \underset{k_4}{\overset{k_3}{\rightleftarrows}} EP_2 \underset{k_6}{\overset{k_5}{\rightleftarrows}} EP \underset{k_8}{\overset{k_7}{\rightleftarrows}} E$$

PPase family II was discovered quite recently (*3*, *4*) and has not yet been characterized in such detail. Remarkably, the active-site structures of family I and family II PPases, including the relative positions of the P_i molecules, metal ions, and the nucleophilic water molecule coordinated with two metal ions, are very similar (*11*, *12*), providing a striking example of convergent evolution. This similarity suggests a common reaction mechanism. However, the catalytic characteristics of family I and II PPases are quite different (*13*). Family II PPases are an order of magnitude more active than family I PPases and exhibit maximal activity in the presence of Mn^{2+}, whereas family I PPases are best activated by Mg^{2+}. In the presence of transition metal ions, family I PPases hydrolyze ATP and a number of other polyphosphates besides PP_i, whereas family II PPases exhibit absolute substrate specificity in the presence of either Mg^{2+} or Mn^{2+} (*13*, *14*). PPases of both families require divalent metal ions for catalytic activity and have multiple binding sites for such ions, but only family II PPases bind metal ions with the affinity characteristic of metalloenzymes (*13*). In family II PPases, the site with the highest binding affinity displays a marked preference for Mn^{2+} over Mg^{2+} (*13*).

Here, we describe the results of a detailed kinetic and thermodynamic study of the family II PPase from *Streptococcus gordonii* (*sg*PPase). We measured the rates of PP_i hydrolysis, PP_i synthesis, and P_i/water oxygen exchange in the presence of Mn^{2+}, Mg^{2+}, and Co^{2+}, as well as the binding affinities for several active-site ligands (metal cofactors, fluoride, and P_i). Then, by comparing these results with those obtained previously for family I PPases, we deduced a kinetic scheme for catalysis by *sg*PPase and explained the differences in the catalytic properties of the two PPase families in terms of rate constants for individual reaction steps.

EXPERIMENTAL PROCEDURES

Enzyme. Expression and purification of *sg*PPase from an overproducing *Escherichia coli* C43(DE3) strain transformed with a suitable plasmid were carried out as described previously (*13*). Metal-free *sg*PPase was prepared by EDTA treatment in combination with ultrafiltration on a Centricon SR30 membrane (30 kDa cutoff). A stock enzyme solution containing 2−5 mM enzyme, 150 mM Tris/Cl buffer (pH 7.2), 1.5 mM $MnCl_2$, and 15 mM $MgCl_2$ was diluted to 100 μM enzyme concentration with 72 mM Hepes/KOH buffer (pH 7.2) containing 28 mM KCl and 2 mM EDTA, and the resulting solution was subjected to three cycles of 20−40-fold concentration/dilution on the Centricon membrane. EDTA concentration in the dilution buffer was 2 mM for the first two cycles and 20−50 mM for the third cycle. After the third cycle, the diluted enzyme solution was incubated with 20−50 mM EDTA for 3 days at 25 °C and finally subjected to six further concentration/dilution cycles with 10 μM EDTA in the dilution buffer. The final solution was adjusted to 1−2 mM enzyme concentration and stored at 4 °C. Enzyme concentration was calculated on the basis of the subunit molecular mass of 33.5 kDa (*13*) and the extinction coefficient $A^{1\%}_{280}$ of 2.62, as determined by active-site titration (see Results).

The magnesium form of *sg*PPase (Mg-*sg*PPase) was prepared by incubating 0.5−1 mM metal-free enzyme with 6.5−8 mM $MgCl_2$ for 3 days at 4 °C in the pH 7.2 buffer containing 0.5 mM EGTA. *sg*PPase containing Mn^{2+} or Co^{2+} in the high-affinity metal-binding site and Mg^{2+} in the other sites (Mn- or Co-*sg*PPase) was prepared by a similar incubation with a 10 μM excess of $MnCl_2$ or $CoCl_2$ over the enzyme concentration (allowing binding of only one transition metal ion per subunit), followed by two concentration/dilution cycles on the Centricon membranes using the buffer containing 10 μM $MnCl_2$ or $CoCl_2$ and three or four concentration/dilution cycles with the buffer containing 10 μM $MnCl_2$ or $CoCl_2$ and 5 mM Mg^{2+}. The final solution was adjusted to 0.5−1 mM enzyme concentration.

Methods. PP_i-hydrolyzing activity was assayed by means of an automatic phosphate analyzer (*15*). PP_i hydrolysis was initiated by addition of the enzxyme to 5−25 mL of otherwise complete reaction medium and monitored for 3−4 min.

Enzyme-bound PP_i formation at equilibrium with medium P_i and initial rates of medium PP_i synthesis were measured luminometrically using a coupled APS-sulfurylase/luciferase system, as described previously (*5*, *16*).

Enzyme-catalyzed [^{18}O]P_i−water oxygen exchange was followed by measurement of the distribution of five [^{18}O]P_i isotopomers containing from zero to four ^{18}O atoms (*17*). The starting P_i, kindly donated by Dr. V. Kasho (University of California, Los Angeles), contained >98% ^{18}O (*18*). The exchange reaction was carried out for 5−15 min in a total volume of 0.05−0.2 mL and stopped by the addition of a 1/5 volume of 1.2 M hydrochloric acid. Samples were lyophilized and stored at −20 °C before mass-spectroscopic analysis. Mass spectra were acquired using an API Q-STAR Pulsar hybrid mass spectrometer (Applied Biosystems, Forster City, CA) equipped with a nano-electrospray ion source (MDS Protana, Odense, Denmark). The nano-electrospray capillaries (MDS Protana) were loaded with 2 μL of sample solution diluted with water to 1−2 mM phosphate concentration. Negative ion mode scanning with the ion spray voltage at −900 V and the instrument settings recommended by Applied Biosystems were used. Fifty scans were routinely acquired and averaged for each sample. A typical mass spectrum, displaying excellent separation of the five P_i peaks, is presented in Figure 1. For more details, see the Results section.

Sedimentation velocity measurements were performed on a Spinco E (Beckman, USA) analytical ultracentrifuge at 48 000 rpm with scanning at 280 nm; the sedimentation coefficient, $s_{20,w}$, was calculated using standard procedures (*19*). The enzyme was preincubated in the appropriate media for at least 1 day before the sedimentation run.

All measurements were performed at 25 °C.

Calculation and Data Analysis. The values of the apparent dissociation constants for the various metal ion complexes used to calculate the free metal ion concentrations at pH 7.2 were as follows: $MgPP_i$, 112 μM (*20*); Mg_2PP_i, 2.84 mM (*20*); $MnPP_i$, 30 μM (*21*); Mn_2PP_i, 130 μM (*22*); $CoPP_i$, 10 μM (*23*); MgEDTA, 0.95 μM (*24*); MgEGTA, 12.3 mM (*24*); CoEGTA, 4 nM (*24*); MnEGTA, 6.5 nM (*24*); CaEGTA, 80 nM (*24*); MnF, 62.5 mM (*25*); CoF, 88.7 mM

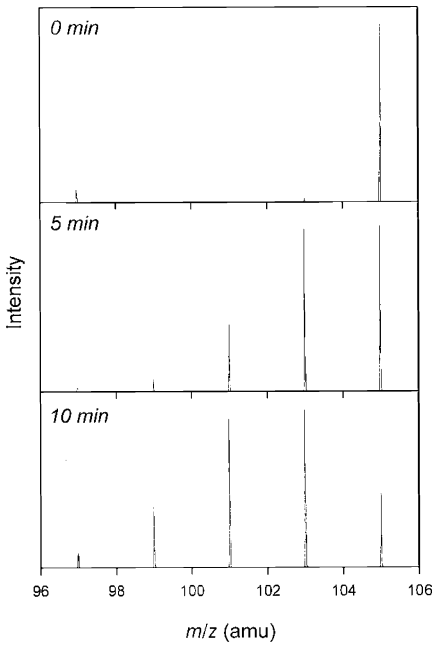

FIGURE 1: Changes in the relative distribution of $[^{18}O]P_i$ isotopomers during P_i−water oxygen exchange catalyzed by Mg-*sg*PPase, as measured by electrospray mass spectrometry. Conditions: 20 mM total potassium phosphate, 5 mM free Mg^{2+}, 4.2 μM PPase, 0.5 mM EGTA, 28 mM KCl, 72 mM HEPES-KOH, pH 7.2; reaction time is indicated on the graphs. The four peaks observed correspond to five P_i isotopomers $P^{16}O_4$, $P^{16}O_3{}^{18}O$, ... $P^{18}O_4$.

(*25*); MgF, 48 mM (*26*); MgP_i, 8.5 mM (*27*); MnP_i, 3.6 mM (*28*); and CoP_i, 9.8 mM (*28*). Where appropriate, these values were derived from published values of the corresponding pH-independent constants.

Nonlinear least-squares fittings were performed using the program SCIENTIST (Micromath), which allows the use of implicit equations.

Metal Ion Binding to sgPPase. Equilibria in the system containing metal ions, *sg*PPase, and chelator (added to buffer free metal ion concentration) are shown in Scheme 2, which is based on previous results (*13*). This scheme shows that metal-ion binding to the high-affinity site shifts the monomer−dimer equilibrium toward the dimer (see also Results). As a consequence, the species EM (monomeric enzyme with bound metal ion) can be neglected. K_M is a microscopic dissociation constant, and $1/2K_M$ and $2K_M$ are the corresponding macroscopic constants for metal binding to two identical sites in the dimer.

The specific activity of *sg*PPase that manifests upon addition of the equilibrium mixture of the enzyme species shown in Scheme 2 to the activity assay medium is given by eq 1

$$A = \frac{2A_0[E_2] + 2A_M[E_2M_2] + (A_0 + A_M)[E_2M]}{[E]_t} \quad (1)$$

where $[E]_t$ is the active enzyme concentration in terms of monomer, and A_0 and A_M are specific activities manifested by enzyme subunit either metal-free (A_0) or metal-bound (A_M) before being added to the assay medium (see Results for more details).

The concentrations of free metal ion and all enzyme species in Scheme 2 and eq 1 were obtained by solving eqs

Scheme 2: Equilibria in the Medium Used to Measure Metal Ion Binding to *sg*PPase[a]

$$\begin{array}{ccccccc} & & K_d & & 1/2K_M & & 2K_M \\ 2E & \rightleftarrows & E_2 & \rightleftarrows & E_2M & \rightleftarrows & E_2M_2 \\ & & K_L & & & & \\ L & \rightleftarrows & LM & & & & \end{array}$$

[a] E, E_2, M, and L are monomer, dimer, metal ion, and chelator, respectively; K_d, K_M, and K_L are dissociation constants.

2−6. The K_d value was fixed at 120 μM, which differs from the value of 93 μM reported previously (*13*) because of a correction made to the enzyme extinction coefficient (see Results).

$$[M]_t = [M] + 2\frac{[M][E]^2}{K_M K_d} + 2\frac{[M]^2[E]^2}{K_M{}^2 K_d} + \frac{[M][L]_t}{K_L + [M]} \quad (2)$$

$$[E] = \frac{K_M\left(\sqrt{K_d(8[E]_t([M] + K_M)^2 + K_d K_M{}^2)} - K_d K_M\right)}{4(K_M + [M])^2} \quad (3)$$

$$[E_2] = \frac{[E]^2}{K_d} \quad (4)$$

$$[E_2M] = 2\frac{[M][E]^2}{K_M K_d} \quad (5)$$

$$[E_2M_2] = \frac{[M]^2[E]^2}{K_M{}^2 K_d} \quad (6)$$

Oxygen Exchange. The rate of ^{18}O exchange between P_i and water (v_{ex}) was calculated using eq 7, where Enr_0 and Enr are the average ^{18}O enrichments of P_i at zero time and time t, respectively. The value of the partition coefficient, P_c, which equals the probability that bound P_i is converted into PP_i rather than released into solution, was calculated from the time-course of the distribution of five P_i isotopomers containing from zero to four ^{18}O atoms, using the program developed by Hackney (*17*). The dependence of the exchange rate on P_i concentration was fit to eq 8, where $k_{ex}[E]_t$ is the value of the exchange rate at infinite P_i concentration, and K_P and K_{P2} are the macroscopic dissociation constants describing binding of the first and the second P_i molecules.

$$v_{ex} = \frac{4[P_i]\ln(Enr_0/Enr)}{t} \quad (7)$$

$$v_{ex} = k_{ex}[E]_t\left(1 + \frac{K_{P2}}{[P_i]} + \frac{K_P K_{P2}}{[P_i]^2}\right) \quad (8)$$

Effect of Fluoride on Enzyme-Bound PP_i. The dependence of the amount of enzyme−PP_i intermediate formed at equilibrium with P_i on the fluoride concentration can be described by Scheme 3, where {E} refers to all enzyme species not having bound PP_i, EPP is the enzyme−PP_i intermediate, F is fluoride, and K_{F1}, K_{F2}, and $K_{F,EPP}$ are the dissociation constants for the corresponding fluoride complexes. Scheme 3 assumes that EPP binds one and {E} binds two fluoride ions.

Scheme 3: Fluoride Binding to *sg*PPase Equilibrated with P_i

$$\begin{array}{ccc} \{E\} & \rightleftarrows & EPP \\ \downarrow\uparrow K_{F1} & & \downarrow\uparrow K_{F,EPP} \\ \{E\}F & & EPPF \\ \downarrow\uparrow K_{F2} & & \\ \{E\}F_2 & & \end{array}$$

Scheme 4: Kinetic Scheme of Catalysis by *sg*PPase

$$E \underset{k_2}{\overset{k_1}{\rightleftarrows}} EPP \underset{k_4}{\overset{k_3}{\rightleftarrows}} EP_2 \underset{k_6}{\overset{k_5}{\rightleftarrows}} EP \underset{k_8}{\overset{k_7}{\rightleftarrows}} E$$

The fraction of enzyme containing bound PP_i in the presence of fluoride (f_{epp}) is given by

$$f_{epp} = \frac{f_{epp0}[E]}{(1 - f_{epp0})[E]_t}\left(1 + \frac{[F]}{K_{F,EPP}}\right) \quad (9)$$

where f_{epp0} is f_{epp} at zero fluoride concentration, [E] and [F] are the concentrations of free enzyme and fluoride, respectively, and $[E]_t$ is the total concentration of enzyme. [E] and [F] are obtained by solving eqs 10 and 11, which are derived from mass conservation equations for enzyme and fluoride, respectively, by expressing the concentration of enzyme and fluoride complexes in terms of [E], [F], f_{epp0}, and the relevant binding constants; $[F]_t$ is the total concentration of fluoride.

$$[E]_t = [E] + \frac{f_{epp0}[E]}{(1 - f_{epp0})}\left(1 + \frac{[F]}{K_{F,EPP}}\right) + \frac{[E][F]}{K_{F1}} + \frac{[F]^2[E]}{K_{F1}K_{F2}} \quad (10)$$

$$[F]_t = [F] + \frac{f_{epp0}[E][F]}{(1 - f_{epp0})K_{F,EPP}} + \frac{[E][F]}{K_{F1}} + 2\frac{[F]^2[E]}{K_{F1}K_{F2}} \quad (11)$$

Fluoride effect on the rate of PP_i hydrolysis (v_h) is described by eq 12 for uncompetitive inhibition, where k_h is the catalytic constant, K_m is the Michaelis constant, and $K_{F,ES}$ is the inhibition constant, characterizing fluoride binding to the enzyme−substrate complex. Eq 12 does not take into account the binding of the second fluoride ion because this binding occurs to an insignificant extent at the low fluoride concentration used in the inhibition measurements.

$$v_h = k_h[E]_t/\left(1 + \frac{K_m}{[PP_i]} + \frac{[F]}{K_{F,ES}}\right) \quad (12)$$

Microscopic Rate Constants. Catalysis by *sg*PPase could be described by Scheme 4, which differs from Scheme 1 by having only one enzyme−PP_i intermediate.

The microscopic rate constants (k_1−k_8) and the equilibrium constants ($K_1 = k_1/k_2$, $K_3 = k_3/k_4$, $K_5 = k_5/k_6$, and $K_7 = k_7/k_8$) for the four reaction steps in Scheme 4 were calculated from the measured catalytic parameters with eqs 13−20 (*16*), where f_{epp}^{lim} and k_s are the values of f_{epp} and $v_s/[E]_t$, respectively, at infinite P_i concentration. Eqs 13−20 are a rearranged form of the equations put forward by Springs et al. (*29*) and Fabrichniy et al. (*16*).

$$K_1 = \frac{k_h}{K_m}f_{epp}^{lim}\left(\frac{1}{k_s} + \frac{4[P_c + f_{epp}^{lim}(1 - P_c)]}{(4 - 3P_c)k_{ex}}\right) \quad (13)$$

$$K_3 = \frac{1 - f_{epp}^{lim}}{f_{epp}^{lim}} \quad (14)$$

$$K_5 = \frac{K_{P2}}{1 - f_{epp}^{lim}} \quad (15)$$

$$K_7 = K_P \quad (16)$$

$$k_1 = \frac{1}{\frac{K_m}{k_h} - \frac{1}{K_1}\left(\frac{1}{K_3k_5} + \frac{1}{k_3}\right)} \quad (17)$$

$$k_3 = \frac{k_{ex}(4 - 3P_c)}{4f_{epp}^{lim}(1 - P_c)} \quad (18)$$

$$k_5 = \frac{k_{ex}(4 - 3P_c)}{4P_c(1 - f_{epp}^{lim})} \quad (19)$$

$$k_7 = \frac{1}{\frac{1}{k_h} - \frac{4[P_c + f_{epp}^{lim}(1 - P_c)]}{(4 - 3P_c)k_{ex}}} \quad (20)$$

RESULTS

Binding Affinities of sgPPase for Different Metal Ions. Family II PPases have one high-affinity and two medium-affinity metal-binding sites per subunit (*13*). The high-affinity site is important for both quaternary structure and catalysis (*13*). Binding of Co^{2+}, Mg^{2+}, and Ca^{2+} to the high-affinity site of *sg*PPase was measured using the approach previously employed to measure Mn^{2+} binding (*13*). This approach makes use of the dependence of enzyme activity on the occupancy of the high-affinity site, which is determined by a combination of two effects. First, metal-ion binding drastically shifts the monomer−dimer equilibrium toward the much more active dimer (*13*). Second, both monomer and dimer are inactive unless the high-affinity site is occupied by a divalent metal ion activator. It is also important that dimer−monomer interconversion is slow on the time-scale of the PPase activity assay.

The binding assay consisted of two steps. First, metal-free enzyme was equilibrated with increasing amounts of a particular divalent metal ion, allowing occupation of a fraction of the available high-affinity sites, and as a consequence, partial dimerization. The incubation medium included a metal chelator (EGTA or EDTA), which helped to maintain a low concentration of free metal ion in the presence of a relatively high enzyme concentration (i.e., it served as a metal buffer). Second, enzyme activity was measured with PP_i as the substrate. The activity assay conditions were carefully selected to maximize the effect of metal binding on activity. Thus, the activities of Mg and Ca enzymes were measured with Mg^{2+} as the activator, giving low A_0 values in comparison to A_M values in eq 1. By contrast, the ratio A_0/A_M was not that favorable when the Co enzyme was assayed with Mg^{2+}; hence, its activity was

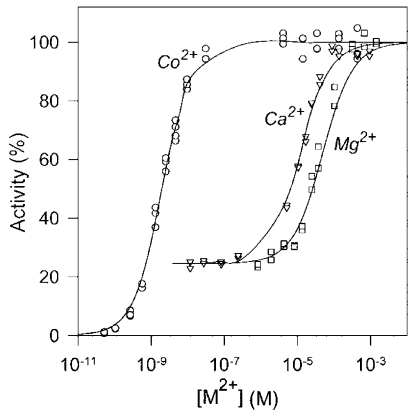

FIGURE 2: Effect of preincubation with different metal ions on *sg*PPase activity. Metal-free enzyme (26 μM) was preincubated for 3−4 days at 25 °C with the chloride salts of the indicated metals in the presence of 40 μM EGTA (Co^{2+} and Ca^{2+}) or EDTA (Mg^{2+}) and 72 mM Hepes/KOH buffer (pH 7.2) containing 28 mM KCl in a total volume of 40 μL. Thereafter, aliquots were withdrawn, and the PPase activity was assayed. The assay medium contained 50 μM PP_i, 150 mM Tris/Cl buffer, pH 7.2 and the following additions: 22 mM $CaCl_2$ and 2 mM EDTA (Co^{2+} incubation) or 20 mM $MgCl_2$ and 0.5 mM EGTA (Mg^{2+} and Ca^{2+} incubations). Longer incubations (5−6 days) resulted in essentially similar activity values, indicating that equilibrium was attained. The lines were obtained with eqs 1−6 using the best-fit parameter values listed in Table 1. The value of A_M is taken as 100% activity for each curve. The abscissa shows the free metal ion concentration in the preincubation medium, as calculated with eqs 2 and 3 using K_M values from Table 1.

assayed with Ca^{2+}, with which A_0 is equal to zero (because metal-free *sg*PPase shows no activity with Ca^{2+} as the cofactor). The activities of metal-free, Mg- and Ca-*sg*PPase preincubated under conditions allowing virtually complete dimerization (high enzyme or metal ion concentration) and assayed with Mg^{2+} were found to be identical. This observation suggests that Mg^{2+} rapidly bound to or replaced Ca^{2+} in the high-affinity site during the activity assay and that the activity measured refers to Mg-*sg*PPase in all these cases. Therefore, the increase in *sg*PPase activity after preincubation with Mg^{2+} or Ca^{2+} is solely due to the shift of the dimer−monomer equilibrium toward the dimer. Accordingly, A_0 was set to A_M in eq 1. By contrast, the activity of Co-*sg*PPase measured with Ca^{2+} or Mg^{2+} was much higher, indicating that bound Co^{2+} was not significantly replaced by Ca^{2+} or Mg^{2+} during the activity assay. This conclusion was supported by the observation that the P_i accumulation curve was linear for at least 0.5 min after enzyme addition to the assay medium.

The dependence of enzyme activity on metal ion concentration in the preincubation mixture displayed two plateau regions for all the metal ions considered, as shown in Figure 2. The plateau at lower metal concentration corresponds to the activity of the 75% monomeric and 25% dimeric enzyme with the assay metal ion bound to the high-affinity site, and the plateau at higher metal concentration corresponds to the activity of predominantly dimeric Co enzyme (Co^{2+} present in the preincubation medium) or Mg enzyme (Mg^{2+} or Ca^{2+} present in the preincubation medium). The binding constants (K_M) derived from the activity-metal concentration curves by fitting eqs 1−6 (Table 2) indicate that the high-affinity site has a much greater preference for transition metal ions over alkali earth metal ions.

Table 1: Parameters Derived from Metal Ion Binding Assays (Figure 2)

metal ion	K_M, nM	A_0, s^{-1}	A_M, s^{-1}
Mn^{2+}	0.20 ± 0.06[a]	270[a]	900[a]
Mg^{2+}	23000 ± 3000 (7000 ± 3000)[b]	210 ± 10	210 ± 10
Ca^{2+}	5400 ± 800	208 ± 5	208 ± 5
Co^{2+}	0.67 ± 0.04	<0.01	94 ± 1

[a] From Parfenyev et al. (*13*). Activity of the enzyme preincubated with Mn^{2+} was assayed with 20 mM Mg^{2+} as the cofactor. [b] Estimated from Mn^{2+} competition experiment.

Table 2: Parameters for P_i−Water Oxygen Exchange Catalyzed by *sg*PPase with Different Metal Ions in the High-Affinity Site

enzyme	$[P_i]$, mM	$v_{ex}/[E]_t$, s^{-1}	P_c
Mg-*sg*PPase	2	0.32 ± 0.01	0.048 ± 0.006
	20	10.3 ± 0.4	0.052 ± 0.006
	50	20 ± 1	0.069 ± 0.006
Mn-*sg*PPase	2	0.75 ± 0.02	0.023 ± 0.017
	20	22 ± 1	0.020 ± 0.011
	50	58 ± 3	0.017 ± 0.016
Co-*sg*PPase	2	0.66 ± 0.02	0.104 ± 0.006
	20	32 ± 1	0.113 ± 0.010
	50	79 ± 1	0.118 ± 0.020

The binding assay also permitted measurement of Mn^{2+} binding to *sg*PPase in the presence of 5 mM Mg^{2+}. In this case, PPase activity was assayed with Ca^{2+} as the activator. The apparent K_M value for Mn^{2+} estimated in this way was 140 ± 20 nM, which is 700 times greater than in the absence of Mg^{2+} (Table 1). The value of K_M for Mg^{2+} can be calculated from this effect as 7 ± 3 μM, assuming a competitive binding mechanism. This value is not much different from the value of 23 μM obtained in the direct binding assay (Table 1).

The sedimentation coefficients ($s_{w,20}$) for *sg*PPase measured in the presence of 0.03 mM Co^{2+} or 0.15 mM Ca^{2+} were 4.0−4.1 S, characteristic of dimeric *sg*PPase (*13*). Previously, we observed similar values of $s_{w,20}$ in the presence of Mn^{2+} and Mg^{2+} and a significantly lower value (3.1 S) in the absence of any metal ion (*13*).

The tightness of Mn^{2+} binding allowed kinetic titration of the high-affinity binding sites in *sg*PPase. In this experiment, *sg*PPase, at a concentration 4 orders of magnitude greater than K_M, was preequilibrated for 10 h with increasing amounts of Mn^{2+} in the absence of any chelator, and enzyme activity was assayed with Ca^{2+} as the activator. The binding site concentration could be easily estimated as the metal ion concentration corresponding to the inflection point in the titration curve (Figure 3). The value of the extinction coefficient for *sg*PPase ($A^{1\%}_{280}$) calculated from the enzyme concentration was 2.62, which differs significantly from the value of 3.43, estimated previously based on the amino acid composition of *sg*PPase (*13*). This discrepancy may be due to the previous method overestimating the extinction coefficient because *sg*PPase contains no Trp residues (*3*, *4*), which make the greatest contribution to protein absorbance at 280 nm.

In the sections that follow, we examined the effect of the nature of the metal ion (Mn^{2+}, Co^{2+}, or Mg^{2+}) bound to the high-affinity site on the catalytic activity of *sg*PPase. All measurements were performed in the presence of 5 mM Mg^{2+}, ensuring that all other available metal binding sites

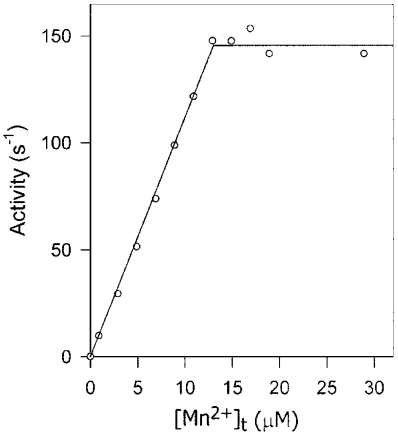

FIGURE 3: Kinetic titration of *sg*PPase active sites. Enzyme concentration was such that the absorbance of its solution at 280 nm in a 1 cm cuvette was 0.115.

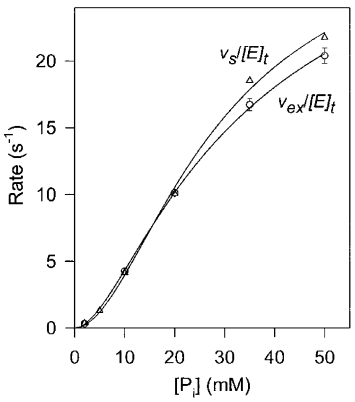

FIGURE 4: Dependence of $v_{ex}/[E]_t$ and $v_s/[E]_t$ on $[P_i]$ for Mg-*sg*PPase. The lines were drawn with eq 8, using the parameter values given in Table 3 (see text for details).

were occupied by Mg^{2+}. In the cases of Mn-*sg*PPase and Co-*sg*PPase, the reaction medium additionally contained 10 μM free Mn^{2+} or Co^{2+}, respectively, to prevent their substitution by Mg^{2+} on the enzyme. At this low concentration, Mn^{2+}, and presumably, Co^{2+} do not bind significantly to other sites (*13*). Further evidence that no leakage of Mn^{2+} or Co^{2+} occurred from the enzyme in these experiments was provided by the observation that the enzyme activity did not vary during the assays and that the corresponding kinetic curves were linear.

P_i−Water Oxygen Exchange. Oxygen exchange has been studied in detail in family I PPases but has not been previously measured in family II PPases. This exchange results from the reversible synthesis of PP_i at the PPase active site; specifically, one P_i oxygen is lost as water during PP_i synthesis, and one is acquired from water during subsequent PP_i hydrolysis. This exchange occurs in only one of the two P_i binding subsites found in the PPase active site. Oxygen exchange is characterized by two parameters: the rate of the exchange (v_{ex}) and the partition coefficient (P_c). P_c is defined as the ratio of the rate at which enzyme-bound P_i loses oxygens and the sum of this rate and the rate of P_i release from the enzyme and can vary between zero and one (*17*).

The oxygen exchange data summarized in Table 2 indicate that the Mg, Mn, and Co forms of *sg*PPase catalyze P_i−water oxygen exchange at rates comparable to that observed with family I PPases (*17*). The value of P_c is, however, severalfold less for *sg*PPase. As noted previously (*29*), the invariance of the P_c value over a wide range of P_i concentrations provides strong evidence that the P_i molecule containing the P atom that was attacked by water during PP_i hydrolysis leaves the active site first, regardless of the nature of the metal ion bound to the high-affinity site. By contrast, this P_i molecule leaves first from the Mg form of yeast (family I) PPase (*29*) but leaves second from the Co, and presumably, Mn forms of this latter PPase (*30*).

Figure 4 shows $v_{ex}/[E]_t$ as a function of P_i concentration for Mg-*sg*PPase. Fitting eq 8 to these data and similar data measured for Mn- and Co-*sg*PPase allowed evaluation of k_{ex} and the P_i binding parameters K_P and K_{P2} (Table 3).

It should be noted that the present work is the first time an ion-spray mass spectrometer has been used to measure the distribution of P_i between its five forms containing different amounts of ^{16}O and ^{18}O. This method does not require any pretreatment of the sample. Earlier analyses made use of electron impact ionization that required conversion of P_i into volatile tris(trimethylsilyl) phosphate prior to analysis (*18*). We found that the two methods give identical results with yeast PPase (data not shown). One problem that was encountered using ion-spray mass spectroscopy was sample contamination with $P(^{16}O)_4$ from the glass capillary holding the sample. This contamination resulted in the $P(^{16}O)_4$ content of the sample being overestimated by 1−5%, depending on the voltage used. However, this problem could be avoided either by using a quartz capillary or by making an appropriate modification to the algorithm of Hackney (*17*) that was used to derive v_{ex} and P_c from the exchange data. Specifically, the percentage contamination was used as an additional unknown parameter. We mainly used the latter approach.

Enzyme-Bound PP_i Formation. A distinctive feature of family I PPases is their ability to form appreciable amounts of enzyme-bound PP_i from medium P_i. At high P_i concentrations, the fraction of enzyme containing bound PP_i (f_{epp}) can reach 20% (*31*). *sg*PPase can also form significant, although much smaller amounts of enzyme-bound PP_i. Thus, f_{epp} was only 0.32 ± 0.02, 0.15 ± 0.01, and 0.19 ± 0.01% at 20 mM P_i for Mg-, Mn-, and Co-*sg*PPase, respectively. Since the dependence of f_{epp} on $[P_i]$ should obey an equation identical to eq 8 but with f_{epp}^{lim} (the limiting value of f_{epp}) in place of $k_{ex}[E]_t$ in the numerator, the values for f_{epp}^{lim} were calculated from the f_{epp} values measured at 20 mM P_i and the K_P and K_{P2} values estimated from the oxygen exchange measurements (Table 3).

PP_i Synthesis in Solution. Although the equilibrium $2P_i \rightleftarrows PP_i$ is markedly shifted toward P_i in water solution, the steady-state rate of medium PP_i synthesis (v_s) could be measured in the presence of excess ATP-sulfurylase, which quantitatively converts the synthesized PP_i into ATP. The latter could be monitored with luciferase (*32*). The dependencies of $v_s/[E]_t$ on $[P_i]$ shown in Figure 4 could be described by a saturation function similar to eq 8 but with k_s (the limiting value of $v_s/[E]_t$) in the numerator and apparent K_P and K_{P2} in the denominator. The k_s values estimated in this way are summarized in Table 3.

Fluoride Binding. Fluoride specifically inhibits family I PPases by replacing the nucleophilic water molecule in the enzyme−substrate complex (*5*, *6*). Consistent with this

Table 3: Catalytic Parameters for $PP_i = 2P_i$ Equilibration by Different Metal Forms of *sg*PPase and by the Magnesium Form of Y-PPase

parameter	Mg-*sg*PPase	Mn-*sg*PPase	Co-*sg*PPase	Y-PPase[a]
k_h, s^{-1}	330 ± 10	3550 ± 70	830 ± 20	260
k_h/K_m, $\mu M^{-1} s^{-1}$	43 ± 4	89 ± 5	73 ± 5	200
K_P, mM	13 ± 3	32 ± 12	26 ± 3	2.7
K_{P2}, mM	28 ± 9	30 ± 10	36 ± 6	3.5
k_{ex}, s^{-1}	34 ± 5	124 ± 30	168 ± 15	170
P_c	0.055 ± 0.004	0.019 ± 0.008	0.117 ± 0.007	0.30
f_{epp}^{lim}, %	1.06 ± 0.25	0.74 ± 0.20	1.00 ± 0.25	16
k_s, s^{-1}	29 ± 5	118 ± 14	140 ± 20	4

[a] Literature values (*37*) recalculated in terms of total PP_i and P_i concentrations, where appropriate.

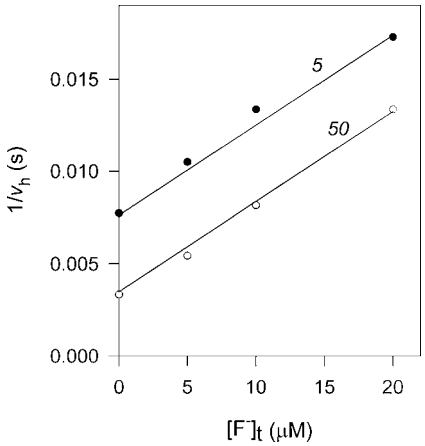

FIGURE 5: Dixon plot of Mg-*sg*PPase inhibition by fluoride. Numbers on the curves refer to PP_i concentration in micromoles per liter. The lines were drawn with eq 12 using the parameter values given in the text.

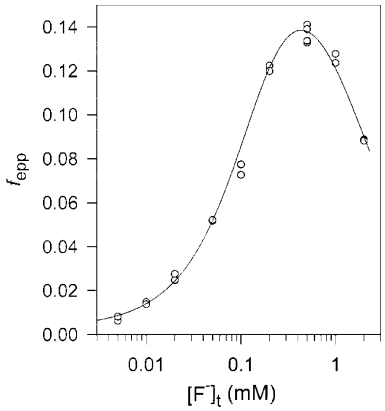

FIGURE 6: Fluoride effect on f_{epp} for Mg-*sg*PPase. Enzyme concentration was 100 μM, and the P_i concentration was 20 mM. The curve shows the best fit to eqs 9−11 and was drawn using the parameter values given in the text.

mechanism, a Dixon plot of the effect of fluoride on the magnesium form of *sg*PPase during steady-state PP_i hydrolysis (Figure 5) points to an uncompetitive inhibition. Qualitatively similar plots were obtained for Mn-*sg*PPase and Co-*sg*PPase, but the inhibition was much weaker, in agreement with the findings of Kuhn et al. (*33*). The values of the inhibition constant $K_{F,ES}$ were found to be 0.0062 ± 0.0003, 8.2 ± 0.6, and >30 mM for Mg-*sg*PPase, Mn-*sg*PPase, and Co-*sg*PPase, respectively.

The enzyme−substrate complex that binds fluoride during steady-state PP_i hydrolysis formally refers to all intermediates following substrate binding (i.e., EPP*, EPP, EP_2, and EP in Scheme 1). To compare the fluoride binding affinities of different intermediates, we investigated the effect of fluoride on f_{epp} in the equilibrium system *sg*PPase-P_i-Mg^{2+}. Fluoride had a dual effect on f_{epp} at fixed P_i: at low fluoride concentrations (<0.2 mM), f_{epp} increased, indicating that EPP* and/or EPP bind fluoride more tightly than any other intermediate; but at high fluoride concentrations, this effect was reversed (Figure 6). The latter observation indicates that some PP_i-lacking intermediate binds fluoride less tightly but with a higher stoichiometry, as shown in Scheme 3 taken from a previous work on family I PPases (*5*), which are affected by fluoride in a very similar manner. The data presented in Figure 6 were fitted to eqs 9−11, yielding the following estimates: $K_{F,EPP} = 1.0 \pm 0.3$ μM, $K_{F1} = 90 \pm 40$ μM, and $K_{F2} = 1200 \pm 500$ μM. These values lead to the following conclusions. (a) The enzyme−PP_i complex binds fluoride much more strongly than the alternative fluoride-binding enzyme species ($K_{F,EPP} \ll K_{F1}$, K_{F2}), consistent with previous data on family I PPases (*5*). (b) The binding constant for EPP, as derived from the equilibrium studies, is less than that for the enzyme−substrate complex derived from the steady-state studies ($K_{F,EPP} < K_{F,ES}$), consistent with the fact that EPP is only one of the intermediates constituting the enzyme−substrate complex. By contrast, $K_{F,EPP} > K_{F,ES}$ for family I PPases (*5*), and this unusual observation formed the basis for the notion that the catalytic reaction of family I PPases involves two enzyme−PP_i intermediates (EPP* and EPP in Scheme 1) with different affinities for fluoride.

Kinetic Scheme and Microscopic Rate Constants. The analysis described next led us to conclude that Scheme 4 is the minimal scheme that adequately describes $PP_i = 2P_i$ equilibration by *sg*PPase. Scheme 4, which has only one enzyme−PP_i intermediate, was originally used to describe catalysis by family I PPases (*29*, *34*, *35*); however, more recent studies (*5*, *9*) have suggested that this process is better described by Scheme 1, which has two enzyme−PP_i intermediates. The microscopic rate constants and the equilibrium constants for the four reaction steps catalyzed by *sg*PPase were calculated from the values of the eight catalytic parameters listed in Table 3 with eqs 13−20. The results of these calculations for different metal forms of *sg*PPase are summarized in Table 4. The experimental errors of k_1 and k_2 for Mg- and Mn-*sg*PPases and of k_7 and k_8 for Mn-*sg*PPase, calculated according to error propagation rules, exceeded the values themselves, allowing only rough estimates of these parameters.

In addition, attempts to use Scheme 1 to describe catalysis by *sg*PPase led to less satisfactory results. First, we found that the equations used to calculate k_4, k_5, and k_6 from the catalytic parameters listed in Table 3, and hence, the

Table 4: Kinetic and Thermodynamic Parameters for Catalysis of $PP_i \rightleftarrows 2P_i$ Equilibration by Different Metal Forms of *sg*PPase and by the Magnesium Form of Y-PPase

parameter	Mg-*sg*PPase	Mn-*sg*PPase	Co-*sg*PPase	Y-PPase[a]
$1/K_1$, μM	60 ± 15	180 ± 60	170 ± 50	0.42−1.08
K_3	90 ± 20	130 ± 40	100 ± 30	4
K_5, mM	28 ± 9	30 ± 10	36 ± 6	2.7
K_7, mM	13 ± 3	30 ± 10	28 ± 3	2.7
k_1, $\mu M^{-1} s^{-1}$	150−600	350−7000	400 ± 200	380
k_2, s^{-1}	4000−30000	60000−1200000	70000 ± 50000	1600−4100
k_3, s^{-1}	3300 ± 900	17000 ± 7000	17000 ± 5000	1400
k_4, s^{-1}	35 ± 5	130 ± 30	175 ± 20	350
k_5, s^{-1}	600 ± 100	6500 ± 3100	1300 ± 200	800
k_6, $mM^{-1} s^{-1}$	20 ± 10	210 ± 130	36 ± 7	300
k_7, s^{-1}	1000 ± 300	7000−35000	2600 ± 600	960−3300
k_8, $mM^{-1} s^{-1}$	70 ± 30	200−1100	100 ± 30	
k_A, s^{-1}				840−2200
k_B, s^{-1}				33−34

[a] From Baykov et al. (*5*).

numerical values for these constants were identical for Schemes 1 and 4. The remaining seven constants were estimated using eq 21, where P_n is one of the eight catalytic parameters found in Table 3 (k_h, k_h/K_m, etc.), and f_n is the analytical expression for the corresponding parameter through the microscopic rate constants k_1, k_2, ... k_8. These constants were treated as unknown parameters, and their values that minimize the function F were obtained using the program SCIENTIST. Two sets of k_1-k_8 were thus obtained, giving nearly identical F values. For both sets, the values of k_4-k_8 were similar to the corresponding values obtained in terms of Scheme 4 (Table 4). Importantly, the values of k_A and k_B were at least 5 orders of magnitude greater than k_3 for both sets, but the ratio k_A/k_B was 10^5 for one set and 10^{-5} for the other set, indicating that one of the enzyme−PP_i intermediates is stoichiometrically insignificant; hence, Scheme 1 can be reduced to Scheme 4.

$$F = \sum_n \left(\frac{P_n - f_n(k_1, k_2, \ldots k_8)}{P_n} \right)^2 \qquad (21)$$

By contrast, using eq 21 with published data for Y-PPase (*5*) confirmed that both enzyme−PP_i intermediates are stoichiometrically significant for this enzyme; moreover, the values of k_1-k_8, k_A, and k_B obtained using this approach were very similar to the values previously obtained by direct calculations (*5*).

DISCUSSION

Metal-Ion Binding. Equilibrium dialysis measurements have revealed that family II PPases contain one high-affinity and two or three low-affinity metal-binding sites for Mn^{2+} and Mg^{2+} per subunit (*13*). The high-affinity site binds Mn^{2+} in the nanomolar range and Mg^{2+} in the micromolar range. The results of the present work confirm those earlier findings and further extend them by showing that Co^{2+} resembles Mn^{2+}, whereas Ca^{2+} resembles Mg^{2+} in their binding to the high-affinity site of *sg*PPase. In addition, *sg*PPase exhibited affinities to Cd^{2+} and Zn^{2+}, similar to or greater than that for Mn^{2+}, but the binding of these cations led to enzyme inactivation (Zyryanov, A. B., unpublished). The high-affinity site in *sg*PPase is thus specific for transition metal ions.

X-ray crystallographic studies of family II PPases from *S. gordonii* (*12*) and *Streptococcus mutans* (*11*) have revealed two enzyme-bound metal ions, M1 and M2, in the enzyme active site (Figure 7). Each of the metal ions has three oxygen ligands from the Asp carboxylates and one nitrogen ligand from the His imidazole. The coordination bond lengths for M1 and M2 are similar, suggesting similar binding strengths. On one hand, this active-site structure explains the high affinity of family II PPases toward transition metal ions, which prefer nitrogen ligands, versus alkali earth metals, which prefer oxygen ligands. But on the other hand, this structure poses a question: why is the stoichiometry of the tight binding only one metal ion per subunit instead of two? A likely explanation is that the second metal ion experiences electrostatic repulsion from the first metal ion bound to the active site. Indeed, the distance between the two metal ions is only 3.6 Å, and they are separated only by a shared water ligand, which presumably acts as a nucleophile. It is therefore possible that the high-affinity site is not associated with only M1 or M2, and the first metal ion to come can bind to the M1 and M2 sites with similar probabilities. In this case, the monometal species in Scheme 2 may be mixtures of two species, one containing M1 and the other M2.

Ca^{2+} alone does not confer activity to family II PPases but can do so provided that the high-affinity site is occupied by Mn^{2+} (*13*). Our binding data rule out the simple explanation that Ca^{2+} does not bind to the high-affinity site strongly enough. Therefore, a reasonable alternative hypothesis is that the high-affinity site is crucial for nucleophilic water activation and Ca^{2+} does not activate water as well as Mn^{2+}, Co^{2+}, or Mg^{2+}. Consistent with this explanation, the pK_a of the aquacomplex is much higher for Ca^{2+} (12.9) than for Mn^{2+} (10.6), Co^{2+} (10.2), and Mg^{2+} (11.4) (*36*). This hypothesis is also supported by the fluoride inhibition data, which indicate that the nature of the metal ion in the high-affinity site is crucial for fluoride binding to *sg*PPase. Although at present there is no direct evidence that fluoride substitutes for nucleophilic water, as occurs in family I PPases (*6*), this seems very likely, given the similarity of the inhibition patterns of the two families.

Mg-sgPPase versus Mg-Y-PPase. Catalysis by family I PPases involves two enzyme−PP_i intermediates (Scheme 1), whereas catalysis by *sg*PPase is adequately described by a scheme containing only one such intermediate (Scheme 4). Two lines of evidence favor Scheme 4 over Scheme 1 for *sg*PPase. First, kinetic simulation experiments using eq 21 indicated that a second enzyme−PP_i intermediate, if any, is kinetically insignificant. Second, the effects of fluoride on *sg*PPase are consistent with a process involving only one such intermediate. Qualitatively, the inhibition patterns are very similar for families I and II when Mg^{2+} is used as the cofactor. Thus, inhibition is quite strong and of an uncompetitive type because fluoride predominantly binds to the enzyme−PP_i complex in both cases. There is, however, one important quantitative difference. In the case of family I PPases, the binding of fluoride to the enzyme−PP_i complex formed from P_i is much weaker than that to the analogous complex formed during steady-state PP_i hydrolysis. This observation, which is incompatible with Scheme 4, provides the most important evidence for the existence of two types of the enzyme−PP_i intermediate, of which only one (EPP* in Scheme 1) binds fluoride (*5*). Simple calculations pre-

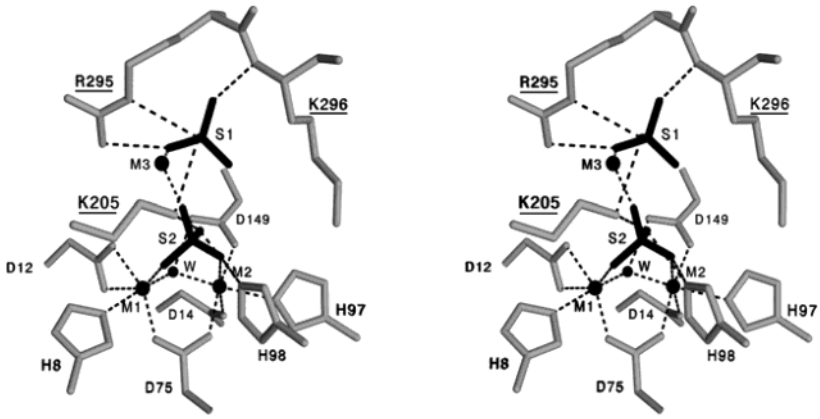

FIGURE 7: Stereoview of the active site in the family II PPase from *S. mutans* (*11*). Three metal ions (M1−M3), the presumable nucleophilic water (W), and two sulfate ions (S1 and S2), mimicking phosphate ions, are shown in black. Residues belonging to the N-domain are underlined. Residue numbering is for *S. mutans* PPase; numbers for *S. gordonii* PPase, whose structure is very similar (*12*), are greater by two.

sented below indicate that this is not the case with *sg*PPase. For Scheme 4, the value of the dissociation constant describing fluoride binding to EPP, as determined from the inhibition of steady-state hydrolysis, should equal the value determined from the fluoride effect on f_{epp}. As shown above, $K_{F,EPP} < K_{F,ES}$, but these constants cannot be directly compared because $K_{F,EPP}$ is a true binding constant whereas $K_{F,ES}$ is an apparent binding constant expressed in terms of total enzyme. To convert $K_{F,ES}$ to a true binding constant, one should multiply it by $f_{epp,ss}$, the fraction of the enzyme−PP_i complex during steady-state hydrolysis at the saturating PP_i concentration. For Scheme 4, $f_{epp,ss}$ is given by eq 22, and based on the values of the rate constants in Table 4, is equal to 0.108. Then, multiplying $K_{F,ES}$ (6.2 μM) by this value, one obtains 0.7 μM, a value close to the value of 1 μM for $K_{F,EPP}$. Thus, Scheme 4 adequately describes both catalysis and fluoride binding to *sg*PPase.

$$f_{epp,ss} = \frac{(k_4 + k_5)k_7}{(k_4 + k_5 + k_3)k_7 + k_3k_5} \qquad (22)$$

The structural difference between EPP and EPP* in family I PPases is not exactly known because high-resolution 3-D structural data are available only for EPP (*6*). The current hypothesis is that they differ in the number of water molecules in the active site (*6*, *37*). This hypothesis is based on X-ray data for Y-PPase showing that metal ions M1 and M2 are separated by two water molecules in the resting enzyme (*8*) and by one (which may be substituted by fluoride) in the enzyme−PP_i and enzyme−$(P_i)_2$ complexes (*6*). It has been suggested that the two water molecules are preserved in the immediate enzyme−PP_i complex (EPP*), but one of them is lost during conversion to EPP (*6*, *37*), making the remaining water molecule, bridging two metal ions, a powerful nucleophile suitably positioned to attack the phosphorus atom of PP_i. Thus, initial PP_i binding by Y-PPase, characterized by a dissociation constant of $k_2/k_1 = 0.41-1.1$ μM, is followed by a favorable conformation change ($k_A/k_B \approx 25-67$), resulting in the overall binding constant (k_2k_B/k_1k_A) of as low as 0.02−0.04 μM.

X-ray crystallographic studies of an EMn_2(sulfate) complex of *sg*PPase (*12*) and an $EMn_3(sulfate)_2$ complex of *S. mutans* PPase (another member of family II) (*11*) revealed that the active-site structures of these family II PPases are very similar to those of family I PPases. These complexes also contain a binuclear metal cluster, and in both complexes there is only one water molecule between M1 and M2 (Figure 7). We speculated that this water molecule is always ready for nucleophilic attack in family II PPases (i.e., there is no intermediate containing two water molecules between M1 and M2 (*11*)). If so, enzyme−PP_i isomerization, which we associate with the release of one water molecule in family I PPases, is not needed in family II PPases.

Further support for this explanation can be found in the overall structures of PPases. In family I PPases, the active site is a preformed structure within a single domain and is ready to bind PP_i. Therefore, further adjustments to generate a catalytically competent structure (e.g., nucleophile generation) should follow PP_i binding. In family II PPase, in contrast, the active site is formed by residues from two domains connected by a flexible hinge. Thus, of the 10 residues forming contacts with the sulfate (P_i analog), metal ions, and nucleophilic water in Figure 7, seven (His8, Asp12, Asp14, Asp75, His97, His98, and Asp149) belong to the N-domain and three (Lys205, Arg295, and Lys296) to the C-domain. These domains can move by tens of angstroms relative to each other, resulting in two quite different conformations of the active site, referred to as open and closed (*12*). Therefore, substrate binding is preceded by a gross conformation change from open to closed, which may involve all changes needed to generate a catalytically competent structure, including nucleophile generation. Considering that this conformational change requires energy, this binding mechanism may also explain the lower affinity of *sg*PPase for PP_i (compare values for $1/K_1 = k_2/k_1$ in Table 4) and phosphate (Table 3) as compared to Y-PPase.

Despite the difference in the kinetic schemes, the rate constants for bound PP_i hydrolysis (k_3) and product release (k_5 and k_7) are similar for the magnesium forms of *sg*PPase and Y-PPase, resulting in similar k_h values (Table 3). However, the K_m value for Mg-*sg*PPase is six times that for Mg-Y-PPase (7.7 vs 1.3 μM), and this difference may reflect much greater value of $1/K_1$ for Mg-*sg*PPase.

Mn- and Co-sgPPase versus Mg-sgPPase. Co-*sg*PPase, and in particular, Mn-*sg*PPase exhibit much higher k_h values than does Mg-*sg*PPase (Table 3), due to their greater values

for k_3, k_5, and k_7 (Table 4). This stands in sharp contrast to family I PPases, in which Mn^{2+} and Co^{2+} dramatically slow product release, and consequently, k_h (*14*). The effect of these transition metal ions on k_3 may be due to the greater polarization of metal-bound nucleophilic water (*36*), whereas the effect on k_5, and probably, k_7 may result from acceleration of the conformational change accompanying product release. PP_i-binding amino acid residues belong to different domains, and if PP_i binding involves a change in enzyme conformation from open to closed, bringing the binding residues together, the hydrolysis of PP_i should effect a backward change to an open conformation with a distorted binding site and low binding affinity. This is consistent with the order in which the two P_i molecules leave the active site. As indicated by the independence of P_c from [P_i] (Table 2), the P_i that contains the oxygen from the water nucleophile leaves the enzyme first, and it is this P_i that has ligands from both domains (Figure 7). The enzyme−PP_i complex thus resembles a loaded spring, whose release is triggered by conversion of PP_i to P_i. The rate of product release is expected to be high for this binding mechanism and to depend on factors that affect the conformational change. Metal ions may be among these factors, but the mechanism by which they might accomplish this role remains to be elucidated.

The value of K_m for Mn-*sg*PPase (40 μM) is five times that for Mg-*sg*PPase (7.7 μM). From eq 17, K_m can be expressed as $K_m = k_h[1 + k_2(1 + k_4/k_5)/k_3]/k_1$, from which it follows that the difference in K_m values may be due to the smaller k_h value for Mg-*sg*PPase, which is not compensated by smaller k_3 and k_5 values (Table 4).

Interestingly, the values of k_h/K_m, which best characterize the catalytic efficiency of a PPase in cell, where the PP_i concentration is expected to be less than K_m, are not much different for Mn-*sg*PPase and Mg-Y-PPase (89 vs 200 μM^{-1} s^{-1}). Moreover, the slightly smaller value of k_h/K_m for *sg*PPase may be compensated by its smaller inhibition by phosphate (see K_P and K_{P2} values in Table 3), whose concentration in cell is in the millimolar range. It should be mentioned in this context that Mn-*sg*PPase is expected to be the predominant form of family II PPases in cell because bacteria containing family II PPases (e.g., *B. subtilis* and *S. mutans*) accumulate Mn^{2+} (*38*, *39*).

ACKNOWLEDGMENT

The authors thank M. V. Turkina and P. V. Kalmykov for their help in this work.

REFERENCES

1. Buttler, L. G. (1971) *The Enzymes* (Boyer, P. D., Ed.) Vol. 4, pp 529−541, Academic Press, New York.
2. Baykov, A. A., Cooperman, B. S., Goldman, A., and Lahti, R. (1999) *Prog. Mol. Subcell. Biol. 23*, 127−150.
3. Young, T. W., Kuhn, N. J., Wadeson, A., Ward, S., Burges, D., and Cook, J. D. (1998) *Microbiology 144*, 2563−2571.
4. Shintani, T., Uchiumi, T., Yonezava, T., Salminen, A., Baykov, A. A., Lahti, R., and Hachimori, A. (1998) *FEBS Lett. 439*, 263−266.
5. Baykov, A. A., Fabrichniy, I. P., Pohjanjoki, P., Zyryanov, A. B., and Lahti, R. (2000) *Biochemistry 39*, 11939−11947.
6. Heikinheimo, P., Tuominen, V., Ahonen, A.-K., Teplyakov, A., Cooperman, B. S., Baykov, A. A., Lahti, R., and Goldman, A. (2001) *Proc. Natl. Acad. Sci. U.S.A. 98*, 3121−3126.
7. Samygina, V. R., Popov, A. N., Rodina, E. V., Vorobyeva, N. N., Lamzin, V. S., Polyakov, K. M., Kurilova, S. A., Nazarova, T. I., and Avaeva, S. M. (2001) *J. Mol. Biol. 314*, 633−645.
8. Heikinheimo, P., Lehtonen, J., Baykov, A., Lahti, R., Cooperman, B. S., and Goldman, A. (1996) *Structure 4*, 1491−1508.
9. Belogurov, G. A., Fabrichniy, I. P., Pohjanjoki, P., Kasho, V. N., Lehtihuhta, E., Turkina, M. V., Cooperman, B. S., Goldman, A., Baykov, A. A., and Lahti, R. (2000) *Biochemistry 39*, 13931−13938.
10. Halonen, P., Baykov, A. A., Goldman, A., Lahti, R., and Cooperman, B. S. (2002) *Biochemistry 41*, 12025−12031.
11. Merckel, M. C., Fabrichniy, I. F., Salminen, A., Kalkkinen, N., Baykov, A. A., Lahti, R., and Goldman, A. (2001) *Structure 9*, 289−297.
12. Ahn, S., Milner, A. J., Futterer, K., Konopka, M., Ilias, M., Young, T. W., and White, S. A. (2001) *J. Mol. Biol. 313*, 797−811.
13. Parfenyev, A. N., Salminen, A., Halonen, P., Hachimori, A., Baykov, A. A., and Lahti, R. (2001) *J. Biol. Chem. 276*, 24511−24518.
14. Zyryanov, A. B., Shestakov, A. S., Lahti, R., and Baykov, A. A. (2002) *Biochem. J. 367*, 901−906.
15. Baykov, A. A., and Avaeva, S. M. (1981) *Anal. Biochem. 116*, 1−4.
16. Fabrichniy, I. P., Kasho, V. N., Hyytia, T., Salminen, T., Halonen, P., Dudarenkov, V. Yu., Heikinheimo, P., Chernyak, V. Ya., Goldman, A., Lahti, R., Cooperman, B. S., and Baykov, A. A. (1997) *Biochemistry 36*, 7746−7753.
17. Hackney, D. D. (1980) *J. Biol. Chem. 255*, 5320−5328.
18. Hackney, D., Stempel, K. E., and Boyer, P. D. (1980) *Methods Enzymol. 64*, 60−83.
19. Chervenka, C. H. (1972) *Methods for the Analytical Ultracentrifuge*, Spinco Division of Beckman Instruments, Inc., Palo Alto, CA.
20. Baykov, A. A., Bakuleva, N. P., and Rea, A. P. (1993) *Eur. J. Biochem. 217*, 755−762.
21. Cooperman, B. S., and Mark, D. H. (1971) *Biochim. Biophys. Acta 252*, 221−234.
22. Pavlov, A. R., Avaeva, S. M., and Baykov, A. A. (1986) *Biokhimiya 51*, 369−377.
23. Smith, R. M., Martell, A. E., and Motekaitis, R. J. (1995) *NIST Critical Stability Constants of Metal Complexes Database (Version 2.0)*, National Institute of Standards and Technology, Gaithersburg, MD.
24. Dawson, R. M. C., Elliott, D. C., Elliott, W. H., and Jones, K. M. (1986) *Data for Biochemical Research*, Clarendon Press, Oxford.
25. Kul'vinova, L. A., Blokhin, V. V., Makashev, Yu. A., and Mironov, V. E. (1981) *Koodinatsionnaya Khimiya 7*, 201−205.
26. Aziz, A., and Lyle, S. J. (1969) *Anal. Chim. Acta 47*, 49−56.
27. Smirnova, I. N., Shestakov, A. S., Dubnova, E. B., and Baykov, A. A. (1980) *Eur. J. Biochem. 182*, 451−456.
28. Zyryanov, A. B., and Baykov, A. A. (2002) *Biochemistry (Moscow) 67*, 635−639.
29. Springs, B., Welsh, K. M., and Cooperman, B. S. (1981) *Biochemistry 20*, 6384−6391.
30. Zyryanov, A. B., Pohjanjoki, P., Kasho, V. N., Shestakov, A. S., Goldman, A., Lahti, R., and Baykov, A. A. (2002) *J. Biol. Chem. 276*, 17629−17634.
31. Janson, C. A., Degani, C., and Boyer, P. D. (1979) *J. Biol. Chem. 254*, 3743−3749.
32. Nýren, C., and Lundin, A. (1985) *Anal. Biochem. 151*, 504−509.
33. Kuhn, N., Wadeson, A., Ward, S., and Young, T. W. (2000) *Arch. Biochem. Biophys. 379*, 292−298.
34. Baykov, A. A., Shestakov, A. S., Kasho, V. N., Vener, A. V., and Ivanov, A. H. (1990) *Eur. J. Biochem. 194*, 879−887.
35. Baykov, A. A., and Shestakov, A. A. (1992) *Eur. J. Biochem. 206*, 463−470.
36. Baes, C. F., Jr., and Mesmer, R. E. (1976) *The Hydrolysis of Cations*, John Wiley, New York.
37. Pohjanjoki, P., Fabrichniy, I. P., Kasho, V. N., Cooperman, B. S., Goldman, A., Baykov, A. A., and Lahti, R. (2001) *J. Biol. Chem. 276*, 434−441.
38. Charney, J., Fisher, W. P., and Hegarty, C. P. (1951) *J. Bacteriol. 62*, 145−148.
39. Martin, M. E., Byers, B. R., Olson, M. O. J., Salin, M. L., Arceneaux, J. E. L., and Tolbert, C. (1986) *J. Biol. Chem. 261*, 9361−9367.

BI0357513